Tellus (1990), *42B*, 481–497

Time constants for the evolution of sea spray droplets

By EDGAR L ANDREAS, *US Army Cold Regions Research and Engineering Laboratory, 72 Lyme Road, Hanover, New Hampshire 03755-1290, USA*

(Manuscript received 29 November 1989; in final form 19 April 1990)

ABSTRACT

Sea spray droplets start with the same temperature as the ocean surface from which they form. In high-latitude, polar-low conditions, they therefore cool and evaporate in a relatively cold wind and may alter the air–sea exchange of heat and moisture. This paper presents equations that model the thermal and size (moisture) evolution of a spray droplet from the time it forms until it reaches equilibrium with its environment. The model does well when tested against some of the scanty data available on the evolution of saline droplets. We parameterize the thermal and size evolution of spray droplets with the time constants τ_T and τ_r, which are, respectively, the times required for a droplet to come to within e^{-1} of its equilibrium temperature and within e^{-1} of its equilibrium radius. τ_r is always about three orders of magnitude larger than τ_T; the thermal exchange is thus complete before the moisture exchange even starts. Consequently, the ambient humidity has little effect on the thermal exchange rate, and the initial droplet temperature has negligible effect on the moisture exchange rate. We also parameterize the gravitational settling of droplets and their potential for turbulent suspension with the time scales τ_f and τ_w, respectively. Comparing the four time scales, we see that spray droplets with initial radii less than 10 μm reach both thermal and size equilibrium with the ambient air. Droplets with initial radii greater than 300 μm, on the other hand, fall back into the sea before exchanging appreciable heat or moisture; they thus have little impact on air–sea exchange. In the mid-range, droplets with initial radii between 10 and 300 μm, the physics is more complex. Even after comparing τ_T and τ_r with τ_f and τ_w, we still cannot say unequivocally which process is fastest because of the rudimentary nature of the τ_w estimates. Future work must thus focus on the generation and turbulent transport of droplets of this size if we are to understand how sea spray affects air–sea exchange.

1. Introduction

When the wind speed at a height of 10 m reaches 3–4 m/s, the ocean surface becomes disrupted; waves break and trap air in the water. Whitecaps form when this air rises to the surface as a bubble cloud and the bubbles burst. These bursting bubbles, in turn, throw sea spray droplets into the air. When the wind reaches a speed of 9 m/s, it is strong enough to tear off the wave crests and blow spray directly into the air (Monahan et al., 1986).

Because sea spray initially has the same temperature as the ocean surface, in high winds spray effectively increases the oceanic surface area and, thus, has the potential for affecting the transfer of all constituents normally exchanged at the air–sea interface. The most important of these constituents are sensible heat, latent heat (or moisture), and gases.

At high latitudes especially, the impact of sea spray on air–sea heat and moisture transfer may be profound. Here the ocean loses enormous amounts of sensible and latent heat when air flowing off the cold pack ice encounters the relatively warm ocean. These fluxes provide energy that generates and maintains polar lows (Rasmussen, 1985; Shapiro et al., 1987; Emanuel and Rotunno, 1989), small synoptic- or sub-synoptic-scale cyclones that form in the ice edge region and intensity as they move over the relatively warm waters of the open ocean (Rasmussen, 1983; Kellogg and Twitchell, 1986; Rasmussen and Lystad, 1987). The high winds associated with polar lows, of course, produce sea spray; this spray, in turn, may feed heat and

moisture back into the storm and further intensify it.

Scientists have recognized the potential for enhanced air–sea transfer due to sea spray for some time (Bortkovskii, 1973, 1987; Borisenkov, 1974; Wu, 1974; Ling and Kao, 1976; Ling et al., 1978; Wang and Street, 1978b; Street et al., 1978; Mestayer and Lefauconnier, 1988; de Leeuw, 1989) but have reached no consensus as to if or when the spray transfer is important or on how to parameterize its magnitude. We, too, are interested in how sea spray impacts air–sea transfer, especially in high-latitude, polar-low conditions. But rather than treating the entire problem of sea spray transfer here, we start with a more focused question: "How do individual sea spray droplets evolve?"

To consider this question, we use equations developed by Pruppacher and Klett (1978) to model the instantaneous temperature and radius of single sea spray droplets from the time they form until they reach equilibrium with their environment. This modeling yields time constants that show how rapidly a spray droplet of initial radius r_0 can exchange heat and moisture with its environment. If the exchange rate is slow, a droplet will probably fall back into the sea before participating fully in the air–sea exchange; if the exchange rate is fast, droplets of radius r_0 will alter the interfacial air–sea exchange if enough are produced. To distinguish between slow and fast, we consider both gravitational settling rates and the effects of turbulence in carrying droplets away from the surface. In light of the spray generation function developed by Monahan et al. (1986), we find that the behavior of spray droplets with radii between 10 and 300 μm will determine whether or not sea spray affects the air–sea transfer. Droplets smaller than 10 μm participate fully in the transfer but carry little of the total spray heat and moisture; droplets larger than about 300 μm fall back to the surface before exchanging enough heat and moisture to be important.

2. Mathematical model

2.1. Size evolution equation

Pruppacher and Klett (1978) developed a rate equation for the change in radius of an aqueous solution droplet [their eq. (13-26)]. Andreas et al. (1981) previously used this equation, which follows, to model condensate droplets:

$$r\frac{dr}{dt}=\frac{D'_w M_w e_{sat}(T_a)}{\rho_s R T_a}\left\{f-\frac{1}{1+\delta}\right.$$
(I)
$$\times\exp\left[\frac{L_v M_w}{R T_a}\left(\frac{\delta}{1+\delta}\right)\right.$$
(II)
$$\left.\left.+\frac{2M_w\sigma_s}{R T_a(1+\delta)\rho_w r}-\frac{v\Phi_s m_s(M_w/M_s)}{(4\pi r^3\rho_s/3)-m_s}\right]\right\}. \quad (2.1)$$
(III) (IV)

Here r is the instantaneous radius of the spray droplet at time t; ρ_s is the density of the droplet; ρ_w, the density of pure water; m_s, the mass of salt in the droplet; and

$$\delta=\frac{T}{T_a}-1=\frac{L_v\rho_s}{T_a k'_a}r\frac{dr}{dt}, \quad (2.2)$$

where T is the instantaneous droplet temperature (assumed uniform) and T_a is the ambient air temperature. Also in (2.1), f is the fractional relative humidity (e.g., if RH = 80%, f = 0.80), $e_{sat}(T_a)$ is the saturation vapor pressure over a pure, flat water surface with temperature T_a, and σ_s is the surface tension of a flat water surface with the same salinity and temperature as the spray droplet. Φ_s is the practical osmotic coefficient of the droplet, and v is the total number of ions into which a salt molecule in the droplet dissociates. Although sea water contains measurable amounts of many dissolved salts, sodium chloride, NaCl, is by far the main component. Henceforth, we assume that spray droplets contain only NaCl as a solute; v is thus 2, and m_s is the mass of NaCl in the droplet. Also in (2.1), D'_w is the molecular diffusivity of water vapor in air, and in (2.2) k'_a is the thermal conductivity of air; both reflect modifications to account for noncontinuum effects. Pruppacher and Klett (1978, p. 416) and Andreas (1989) showed that using these modified quantities, rather than just the bulk diffusivity and the bulk conductivity, is necessary. Finally, in (2.1) R is the universal gas constant, L_v is the latent heat of vaporization of water, and M_w and M_s are the molecular weights of water and of NaCl, respectively.

The nomenclature table in the appendix lists all of these symbols and gives the values of the ones that are constants. See Andreas (1989) for a more thorough description of the model.

In (2.1) we see that four distinct phenomena affect the diffusion of water vapor at the surface of a sea spray droplet. Term (I), the ambient humidity, is the main term driving the diffusion. This, compared with the humidity at the surface of the droplet, dictates in which direction the vapor diffuses. Terms (II), (III), and (IV) predict that surface humidity. Term (II) results because the droplet is not at the ambient air temperature; therefore, its surface vapor pressure is computed at T rather than at T_a. Term (III) contains the effects of surface tension. An increase in this term increases the vapor pressure at the droplet surface and thereby enhances evaporation but retards condensation. Notice the r^{-1} dependence: smaller droplets suffer larger effects because of this term. Term (IV) results because salts dissolved in the droplet depress its surface vapor pressure.

Since $|\delta|$ is rarely larger than 0.1, in (2.1) we can approximate

$$\frac{1}{1+\delta} \approx 1-\delta, \tag{2.3}$$

$$\exp\left[\frac{L_v M_w}{RT_a}\left(\frac{\delta}{1+\delta}\right)\right] \approx 1+\frac{L_v M_w \delta}{RT_a}, \tag{2.4}$$

and

$$\frac{2M_w\sigma_s}{RT_a(1+\delta)\rho_w r} \approx \frac{2M_w\sigma_s}{RT_a\rho_w r}. \tag{2.5}$$

Thus, (2.1) becomes

$$r\frac{dr}{dt} = \frac{D'_w M_w e_{sat}(T_a)}{\rho_s RT_a} \times\left[f-(1-\delta)\left(1+\frac{L_v M_w \delta}{RT_a}\right)\exp y\right], \tag{2.6}$$

where

$$y = \frac{2M_w\sigma_s}{RT_a\rho_w r} - \frac{\nu\Phi_s m_s(M_w/M_s)}{(4\pi r^3\rho_s/3)-m_s}. \tag{2.7}$$

Since solute and surface tension effects are small for many spray droplets in the size range that we will consider (Pruppacher and Klett, 1978, p. 420), y is small. Therefore, we also approximate

$$\exp y \approx 1+y. \tag{2.8}$$

Substituting this in (2.6), discarding second and higher order terms, then realizing that δ also contains $r(dr/dt)$, we rearrange (2.6) to obtain the rate of change of the spray droplet radius,

$$\frac{dr}{dt} = \frac{[(f-1)-y]r^{-1}}{\dfrac{\rho_s RT_a}{D'_w M_w e_{sat}(T_a)} + \dfrac{L_v\rho_s}{T_a k'_a}\left(\dfrac{L_v M_w}{RT_a}-1\right)}. \tag{2.9}$$

Implicit in this result is the condition for a droplet to be in moisture equilibrium with its environment. This occurs when

$$f-1=y. \tag{2.10}$$

Thus, the relative humidity is the key to determining the equilibrium radius, although the mass of salt contained in the droplet m_s, the air temperature T_a, and the droplet temperature T, which affect ρ_w, ρ_s, and σ_s, are also important. Andreas (1989) explained how to compute the physical and chemical parameters in (2.9).

2.2. *Thermal evolution equation*

Pruppacher and Klett (1978) also developed a rate equation for the change in temperature of an aqueous solution droplet. Their result, eq. (13-64), is

$$\frac{d}{dt}(T_a-T) = \frac{-3}{r^2\rho_s c_{ps}}[k'_a(T_a-T) + L_v D'_w(Q_a-Q_r)], \tag{2.11}$$

where we have set the ventilation coefficients equal to 1. In (2.11), c_{ps} is the specific heat of a sea spray droplet at constant pressure, and Q_a and Q_r are the ambient vapor density and the vapor density at the droplet surface, respectively.

We assume that the air at the droplet surface is in vapor equilibrium with the droplet. Thus (Pruppacher and Klett, 1978, p. 141),

$$Q_r = \frac{100M_w e_{sat}(T)}{RT}\exp y, \tag{2.12}$$

where $\exp y$ is the relative humidity at the droplet surface, and the 100 is necessary to give Q_r in kg/m^3 when e_{sat} is in hPa.

Pruppacher and Klett (1978) assumed that the temperature within a droplet is uniformly T. This is a crucial assumption but an accurate one. We

can show it to be valid by assuming that there is no fluid motion within a droplet and then using the solution that Carslaw and Jaeger (1959, pp. 233–234) gave for heat flow in a solid sphere. They showed that the time required for a sphere of radius r to be everywhere within 4% of an impulsively applied surface temperature is

$$\tau_h = \frac{0.4r^2}{D_h}, \tag{2.13}$$

where, in our case, $D_h = 1.4 \times 10^{-7}$ m^2/s is the diffusivity of heat in sea water at 0°C (Horne, 1969, p. 56). For 1-μm droplets, $\tau_h = 2.9 \times 10^{-6}$ s; for 100-μm droplets, $\tau_h = 2.9 \times 10^{-2}$ s. Later, when we present the time constants τ_T that characterize the time required for droplets to reach equilibrium in air at temperature T_a, we will see that τ_T is always about 20 times larger than τ_h. Of course, if we allow fluid motion in the droplets, τ_h would be even less than predicted by (2.13). Thus, spray droplets are always well mixed with respect to temperature.

2.3. *Model tests*

To model the thermal and size evolution of sea spray droplets, we integrated (2.9) and (2.11) simultaneously using a multi-step Euler method with a predictor-corrector technique (Andreas, 1989). The time steps were logarithmic.

In doing this integration, we found that the droplet temperature always reaches its equilibrium value T_{eq} long before the droplet reaches its equilibrium radius. According to (2.11), thermal equilibrium exists when

$$T_{eq} = T_a + \frac{L_v D'_w}{k'_a}(Q_a - Q_r). \tag{2.14}$$

Since D'_w, k'_a, and Q_r depend on the droplet radius, T_{eq} changes slowly as the radius changes, though the droplet is in virtual thermal equilibrium with its environment. To model these equilibrium temperature changes, we computed the equilibrium temperature at time step $n+1$ from

$$T_{n+1} = \frac{1}{2}\left\{T_n + T_a + \frac{L_v(T_n) D'_w(T_n, r_{n+1})}{k'_a(T_n, r_{n+1})} \times [Q_a - Q_r(T_n, r_{n+1})]\right\}, \tag{2.15}$$

where T_n is the equilibrium temperature at time step n, and r_{n+1} is the droplet radius at time step $n+1$. The averaging precludes numerical instabilities.

To test the equations that Pruppacher and Klett (1978) developed, our evaluations of the physical and chemical variables involved, and the numerical method, we compared the data of El Golli et al. (1974) and Ranz and Marshall (1952) with model predictions (Figs. 1–4). El Golli et al. observed the evaporation of saline droplets as an air stream carried them through a pipe in which temperature and humidity were controlled. Although the droplets that El Golli et al. observed had initial radii near the median of sea spray droplets, about 8 μm, their other experimental parameters were not especially representative of a sea spray environment. Typically, the surface salinity of the ocean S is about 34‰, and the ambient relative humidity is 80% or higher. Though El Golli et al. observed droplets in an environment with RH = 80%, the initial salinity for these was only 2‰ (Fig. 3). In their highest salinity case, $S = 29$‰, the relative humidity was only 29% (Fig. 1). Fortunately, nothing in our model equations makes them applicable only to the higher salinity sea spray environment; they should also be accurate at lower salinity.

We must, however, be careful in treating low-humidity cases. At low humidity, a droplet may lose enough water by evaporation to become

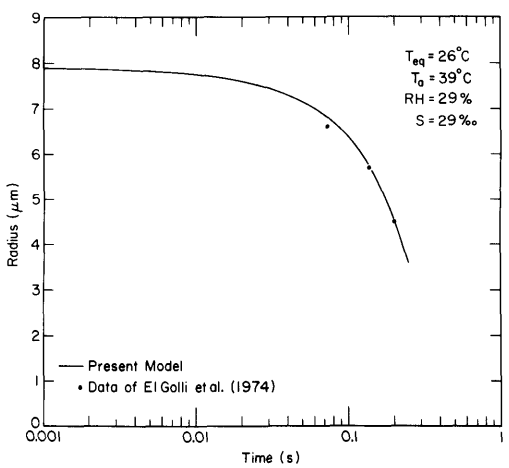

Fig. 1. Model results compared with data from Table 2 in El Golli et al. (1974). Model conditions are RH = 29%, $S = 29$‰, $T_{eq} = 26$°C, $T_a = 39$°C, and $P = 1000$ hPa.

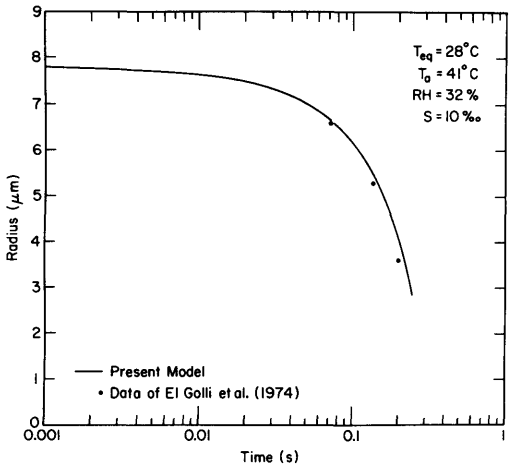

Fig. 2. Model results compared with data from Table 3 in El Golli et al. (1974). Model conditions are RH = 32%, $S = 10‰$, $T_{eq} = 28°C$, $T_a = 41°C$, and $P = 1000$ hPa.

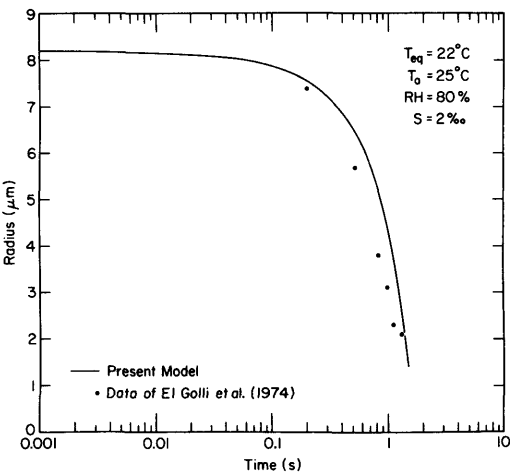

Fig. 3. Model results compared with data from Table 4 in El Golli et al. (1974). Model conditions are RH = 80%, $S = 2‰$, $T_{eq} = 22°C$, $T_a = 25°C$, and $P = 1000$ hPa.

saturated with salt. At 0°C, one liter of pure water can dissolve 0.357 kg of NaCl; thus, the maximum molality of a saline solution is 6.11. Such a saturated solution droplet is in moisture equilibrium with air having a relative humidity of about 75% (Twomey, 1954). At lower humidity,

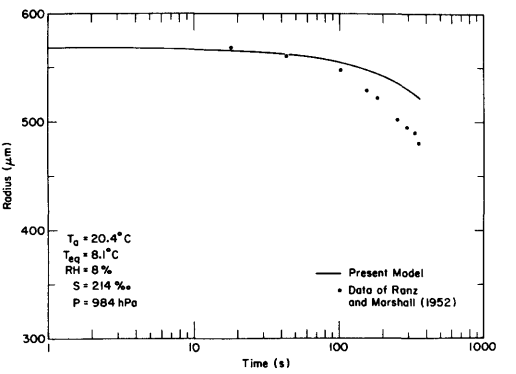

Fig. 4. Model results compared with data from Fig. 15b in Ranz and Marshall (1952). Model conditions are RH = 8%, $S = 214‰$, $T_{eq} = 8.1°C$, $T_a = 20.4°C$, and $P = 984$ hPa.

the water will eventually evaporate and the salt will crystallize. For the two low-humidity data sets collected by El Golli et al. (1974) (Figs. 1, 2), we therefore stopped the calculations when evaporation raised the droplet molality to 6.11.

Another minor problem was that El Golli et al. (1974) reported only one "average" temperature for each set of experimental conditions but did not explain what this average was. In running our model, we therefore varied T_a and T_w (the initial droplet temperature) to get the best agreement with their data. It turned out that, in our notation, their "average" temperature is T_{eq}, the droplet temperature at equilibrium.

Aside from Fig. 3, where our model overestimates the experimental droplet size by about 30%, on average, the model computations agree quite well with the size evolution data collected by El Golli et al. (1974).

Data presented graphically by Ranz and Marshall (1952, their Fig. 15b) provide another important test of our model. Although Ranz and Marshall studied large and unnaturally saline droplets ($S = 214‰$), our model simulates their data well. Fig. 4 shows that the model is always within 9% of their data. Ranz and Marshall did not report the ambient relative humidity for their experiment but stated that it was near zero. By trial and error, we found that a relative humidity of 8% produced the best agreement between modeled values of T_{eq} and the droplet temperatures measured by Ranz and Marshall.

Our successful simulation of the Ranz and Marshall (1952) data substantiates some of the fundamental physics in the model. Cheng et al. (1988) recently reported that they had produced hollow, spherical, salt particles by evaporating sea water droplets and noted that Ranz and Marshall had observed similar evaporative particles. Cheng et al. speculated that the hollow spheres might form because sea salts have low diffusivity in water and, thus, would concentrate at the surface of evaporating droplets. If this mechanism is, indeed, at work, our model would be suspect; it assumes that the salt within the droplet is well mixed. Model simulations of the Ranz–Marshall data, however, refute this mechanism and, thus, confirm that the salt is well mixed. In their Fig. 15b, Ranz and Marshall noted that the first salt crystals began forming at about 380 s after the droplet formed. In our simulation of their data, the droplet reached salt saturation, a molality of 6.11, near 390 s. (In Fig. 4, we plot no data or model results beyond this limit.) This excellent agreement supports our assumption that the salt in the droplets is well mixed. For if salt were concentrating and crystallizing near the evaporating surface as Cheng et al. hypothesized, Ranz and Marshall should have observed crystals forming much earlier.

Using an analysis similar to the one that led to (2.13), we can look more closely at the hypothesis that salt diffusion in an evaporating droplet is so slow that salt concentrates near its surface. Salt diffusion in a sphere is analogous to heat diffusion in a sphere: an incremental surface evaporation is equivalent to an incremental injection of salt at the droplet surface. This salt will diffuse throughout the droplet by molecular processes. But unlike the heat diffusion problem, in which the surface is clamped at the new temperature, the salt will become diluted as it diffuses in the sphere; the final concentration will, therefore, be everywhere less than the original surface concentration. Consequently, a time constant like (2.13) will be an upper bound on the time required (τ_s) for salt injected at the surface to diffuse throughout the droplet. That is,

$$\tau_s < \frac{0.4r^2}{D_s}, \tag{2.16}$$

where $D_s = 6.8 \times 10^{-10}$ m^2/s is the molecular diffusivity of NaCl in sea water at 0°C (Horne, 1969, p. 56). For 1-μm droplets, $\tau_s < 5.9 \times 10^{-4}$ s; for 100-μm droplets, $\tau_s < 5.9$ s. Computations that we will discuss later show that these diffusion times are always two orders of magnitude less than the time constants τ_r, which characterize how rapidly sea spray droplets evaporate. Therefore, salt diffusion within sea spray droplets always seems to be fast enough to maintain a well-mixed interior during evaporation in a typical marine environment.

3. The generation of sea spray

Information on the generation rate of sea spray droplets in a given size range comes from many sources. Monahan (1968), Preobrazhenskii (1973), Monahan et al. (1983), Wu et al. (1984), and de Leeuw (1986a, 1986b, 1987) measured the spray droplet size distribution at the sea surface. Wu (1973), Lai and Shemdin (1974), Wang and Street (1978a), Mestayer and Lefauconnier (1988), and Mestayer et al. (1989) measured the spray size distribution in wind-wave tunnels. Monahan et al. (1982) measured it in a whitecap simulation tank.

Monahan et al. (1986) synthesized much of these data in a single spray generation function by recognizing that two mechanical processes produce sea spray. As the bubbles in whitecaps rise to the surface and burst, they produce *film* and *jet* droplets (Blanchard, 1963, 1983; Cipriano and Blanchard, 1981; Woolf et al., 1987; Blanchard and Syzdek, 1988). When the 10-m wind exceeds a speed of about 9 m/s, it can tear off the wave crests and produce the larger *spume* droplets (Monahan et al., 1983). Monahan et al. (1986), thus, wrote the spray generation function dF/dr_{80} as the sum of two terms,

$$\frac{dF}{dr_{80}} = \frac{dF_0}{dr_{80}} + \frac{dF_1}{dr_{80}}. \tag{3.1}$$

Here dF/dr_{80} is the number of droplets produced per unit surface area per second per micrometre increment in droplet radius, and dF_0/dr_{80} and dF_1/dr_{80} are the contributions from bubbles and from spume droplets, respectively. In (3.1), r_{80} is the droplet radius converted to an ambient relative humidity of 80%. See Monahan et al. (1986) or Andreas (1989) for the functional forms of dF_0/dr_{80} and dF_1/dr_{80}.

Because we want to track the evolution of spray droplets from the instant they form, a spray generation function in terms of r_{80} is inadequate. From dF/dr_{80} we can, however, find dF/dr, the spray generation function in terms of the droplet radius at formation r_0, from

$$\frac{dF}{dr} = \frac{dr_{80}}{dr_0}\frac{dF}{dr_{80}}. \tag{3.2}$$

To find dr_{80}/dr_0, we used Fitzgerald's (1975) results for the equilibrium size of various solution droplets at arbitrary relative humidity [e.g., Fairall et al. (1983)]. Andreas (1989) reported our results for $S = 34‰$ and for r_0 between 0.1 and 500 μm,

$$\frac{dr_{80}}{dr_0} = 0.5049 r_0^{-0.0244}. \tag{3.3}$$

Using (3.1–3.3) and the dF_0/dr_{80} and dF_1/dr_{80} functions given by Monahan et al. (1986), we estimated the rate at which spray droplets form as a function of wind speed. On multiplying this number flux by the initial volume of the droplets, $(4/3)\pi r_0^3$, we calculated the volume flux (Fig. 5), since this flux is what really determines the heat- and moisture-carrying capacity of the spray. Not unexpectedly, the volume of droplets produced at a given radius increases monotonically with the 10-m wind speed. This is the bursting bubble mechanism. Fig. 5 shows also that at a wind speed of about 9 m/s a new spray generation mechanism becomes effective. This is spume generation.

The purpose of this section is to identify the size range of spray droplets with which we must be concerned. Although Burk (1984) and Stramska (1987) suggested that (3.1) predicts too many spume droplets, and work that we will report elsewhere confirms this, Fig. 5 is, nevertheless, accurate enough to delineate that size range. We can call $r_0 = 0.5$ μm a lower limit, because the volume of the small droplets becomes negligible when compared to the peak in the volume flux. A reasonable upper limit is $r_0 = 500$ μm, because, as we will show later, 500-μm droplets remain in the air less than a second before falling back into the sea. Henceforth, we will limit our discussion of sea spray to droplets with initial radii between 0.5 and 500 μm.

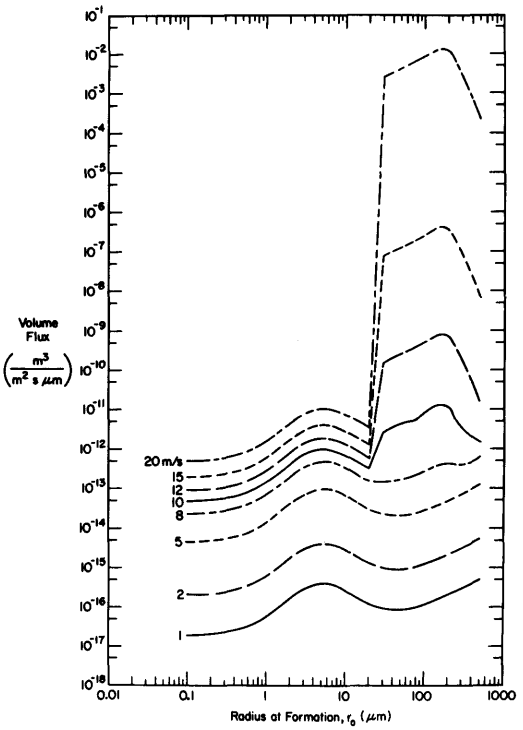

Fig. 5. The spray volume flux for various values of the 10-m wind speed, computed from the spray generation function (3.2) developed by Monahan et al. (1986).

Fig. 5 makes another important point. The increase at higher wind speeds in the volume of droplets with radii greater than 10 μm can potentially overwhelm the thermodynamic effects due to the smaller droplets, despite their longer atmospheric residence times. Thus, it will be crucial to understand the fate of 10- to 300-μm droplets well if we are to understand how sea spray affects air–sea heat and moisture exchange. We will return to this point later.

4. Examples of droplet evolution

The environmental parameters that we will use for computing the thermal and size evolution of sea spray droplets reflect polar-low conditions. The surface salinity S of the high-latitude ocean is commonly about 34‰; the sea surface temperature T_w is typically 0°C. If the wind is

blowing off the pack ice, the air temperature T_a may be as low as $-20°C$. For a southerly wind, the air is warmer; it could reach, say, 5°C. For completeness, we will also consider an air temperature typical of lower latitudes, 20°C. Computations at $T_a = 20°C$, $T_w = 0°C$, and $S = 34‰$ lead to no unnatural results because the size evolution of spray droplets depends negligibly on T_w and only weakly on S for typical open ocean values.

4.1. Thermal evolution

Fig. 6 shows three plots of the evolution of the droplet temperature T. The spray droplet always started at the temperature of the surface water, T_w. T_{eq} is the equilibrium temperature of the droplet in the specific environment and is given by (2.14). Fig. 6 shows the nondimensional temperature $[T(t) - T_{eq}]/[T_w - T_{eq}]$ as a function of the nondimensional time t/τ_T, where τ_T is the time required for the spray droplet to reach e^{-1} of its equilibrium value. That is,

$$\frac{T(\tau_T) - T_{eq}}{T_w - T_{eq}} = e^{-1}. \tag{4.1}$$

In Section 5, we will quantify τ_T.

The thermal evolution depicted in Fig. 6 depends negligibly on the relative humidity. Spray droplets reach thermal equilibrium so quickly that no mass has yet been exchanged.

The three droplets in Fig. 6 have nearly identical thermal evolution curves. Thus, the nature of thermal transfer from a sea spray droplet does not depend strongly on its size, on its initial temperature, or on the ambient temperature and humidity. It does not even depend much on the direction of the transfer. In Fig. 6c the droplet is warming, and the nondimensional temperature generally falls below the line

$$\frac{T(t) - T_{eq}}{T_w - T_{eq}} = \exp(-t/\tau_T). \tag{4.2}$$

Although the nondimensional temperature is above this line for the two cooling cases, Figs. 6a and 6b, deviations from $\exp(-t/\tau_T)$ are not large. Consequently, if we know τ_T and T_{eq}, which we do from (2.14), $\exp(-t/\tau_T)$ is a fairly accurate model for the thermal evolution of spray droplets, regardless of the environmental conditions (see also Pruppacher and Klett, 1978, p. 447).

4.2. Size evolution

Fig. 7 shows three examples of spray droplet size evolution. Note that Figs. 6a and 7a are for the same set of environmental conditions. In Fig. 7, we plot the nondimensional radius $r(t)/r_0$, where r_0 is the initial radius, versus the nondimensional time t/τ_r. The time constant τ_r is defined analogously to τ_T; τ_r is the time required

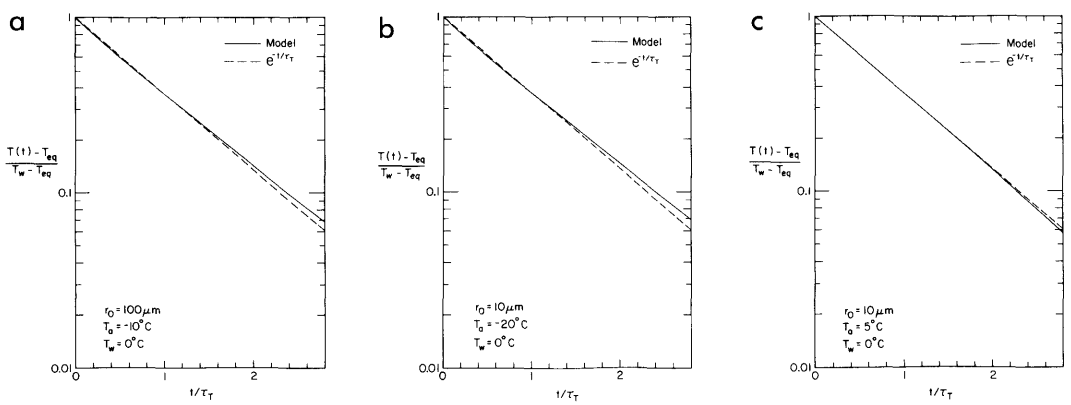

Fig. 6. Model computations of the thermal evolution of spray droplets. Environmental conditions are $T_w = 0°C$, $S = 34‰$, and $P = 1000$ hPa; and in (a) $r_0 = 100\ \mu m$, $T_a = -10°C$; in (b) $r_0 = 10\ \mu m$, $T_a = -20°C$; in (c) $r_0 = 10\ \mu m$, $T_a = 5°C$.

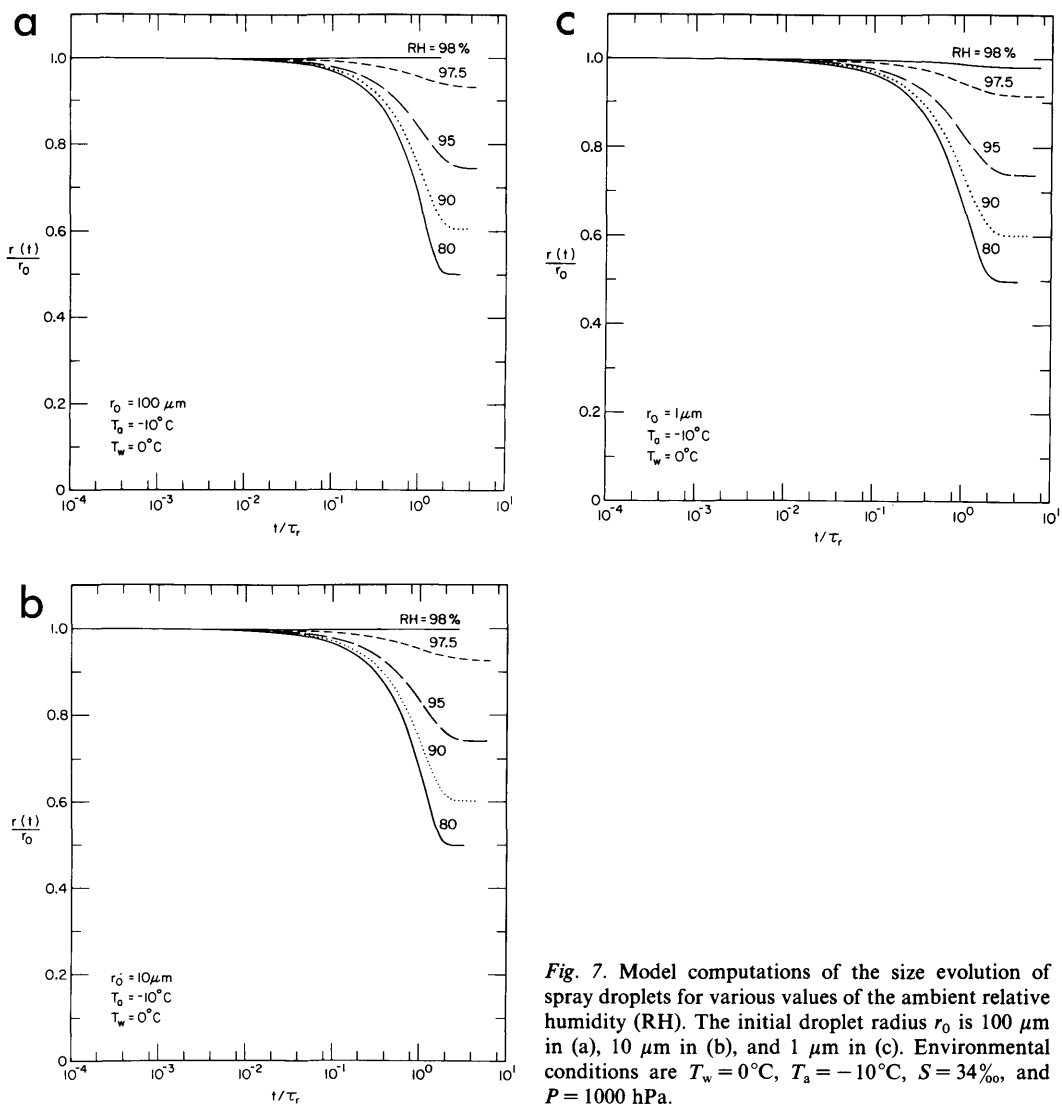

Fig. 7. Model computations of the size evolution of spray droplets for various values of the ambient relative humidity (RH). The initial droplet radius r_0 is 100 μm in (a), 10 μm in (b), and 1 μm in (c). Environmental conditions are $T_w = 0°C$, $T_a = -10°C$, $S = 34‰$, and $P = 1000$ hPa.

for a spray droplet to come to within e^{-1} of its equilibrium radius r_{eq}. That is,

$$\frac{r(\tau_r) - r_{eq}}{r_0 - r_{eq}} = e^{-1}. \tag{4.3}$$

In Section 5 we will present τ_r values.

The three plots in Fig. 7 are nearly identical and thus demonstrate that, when we non-dimensionalize $r(t)$ with r_0 and time with τ_r, the nature of spray droplet size evolution depends almost solely on the ambient relative humidity. One exception to this generalization, however, is the RH = 98% case. The 10-μm and 100-μm droplets grow slowly in an environment with RH = 98%; the 1-μm droplet evaporates slowly when RH = 98%. The relative size of the surface tension term, Term (III) in (2.1) or the first term on the right-hand side of (2.7), is responsible for this effect. For small radii, this term can make y larger than -0.02 and thus change the direction of vapor diffusion at the droplet surface [see (2.10)].

Fig. 7 also suggests why Fairall et al. (1983) and Monahan et al. (1986) found r_{80}, the equilibrium spray droplet radius at 80% relative humidity, to be such a convenient standard. When a droplet reaches equilibrium in an environment with RH = 80%, $r_{80} = r_0/2$.

5. Time constants

The time constants τ_T and τ_r parameterize how quickly a sea spray droplet comes to equilibrium with its environment. With our model we can compute τ_T and τ_r for any initial radius and for any set of ambient conditions with RH > 75%. Fig. 8 shows plots of τ_T and τ_r for droplets with initial radii from 0.5 to 500 μm and for various ambient conditions. Note the τ_T and τ_r values. A 1-μm droplet is within e^{-1} of its equilibrium temperature in less than 10^{-4} s; a 100-μm droplet, in less than 1 s. A 1-μm droplet is within e^{-1} of its equilibrium radius in about 0.5 s; a 100-μm droplet, in about 1000 s. Clearly, the time constants depend on the droplet radius and on the constituent being exchanged.

The τ_T line in each plot of Fig. 8 depends negligibly on the humidity; we thus found no need to mention in the caption the humidity used for the τ_T calculations. Fig. 8 itself explains this lack of humidity dependence. Because τ_T is about three orders of magnitude less than τ_r, moisture exchange at the droplet surface can have no effect on the thermal exchange: a droplet reaches thermal equilibrium long before moisture diffusion begins in earnest at its surface. Consequently, because a droplet reaches thermal equilibrium with the air long before moisture transfer begins, the initial droplet–air temperature difference can have no effect on that transfer. Hence, the choice of T_w is immaterial in the size evolution computations.

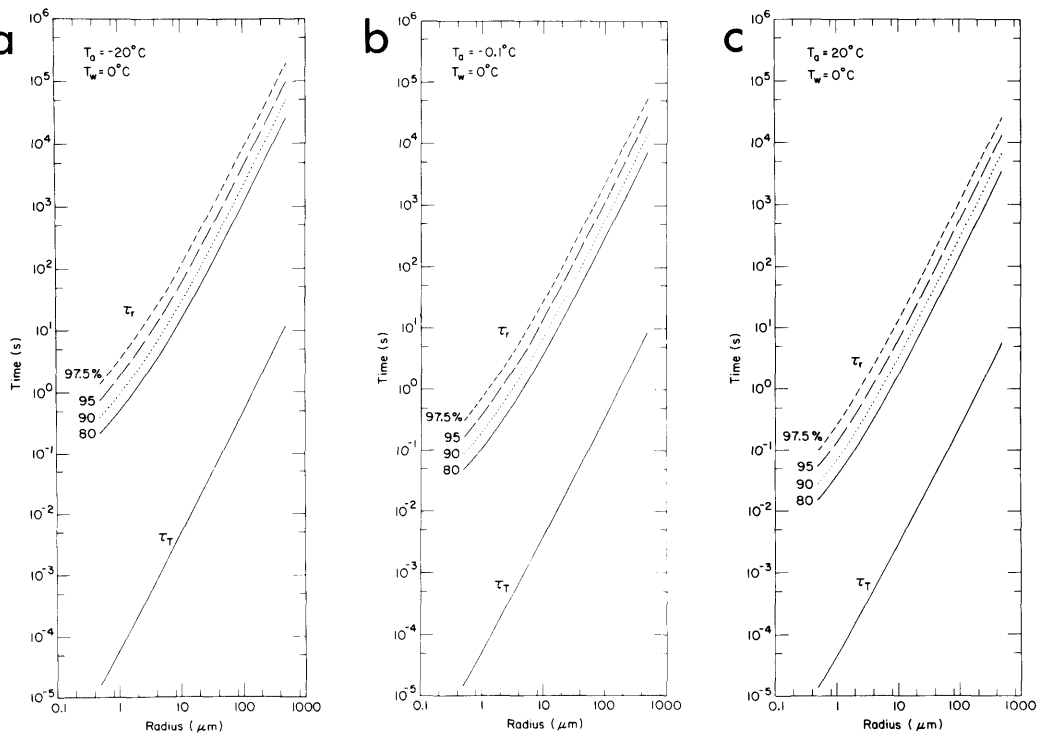

Fig. 8. Time constants for the thermal (τ_T) and size (τ_r) evolution of sea spray droplets plotted versus the initial radius. Numbers on τ_r show the ambient relative humidity. Other environmental conditions are $T_w = 0$°C, $S = 34$‰, $P = 1000$ hPa, and in (a) $T_a = -20$°C, in (b) $T_a = -0.1$°C, and in (c) $T_a = 20$°C.

τ_T also depends only weakly on the air temperature T_a. In Fig. 8, τ_T decreases by a factor of only about 2 as T_a increases from $-20°$ to 20°C. This temperature effect is due strictly to the temperature dependence of the thermodynamic constants in (2.11).

In each plot in Fig. 8, τ_r increases as the relative humidity increases. The reason is obvious from (2.9): the larger $|f-1|$ is, the faster the radius changes.

We have ordered the individual plots in Fig. 8 such that 8a has the largest value of τ_r at a given radius and relative humidity and 8c has the smallest. This sequence also corresponds to air temperatures that go $-20°$, $-0.1°$, and 20°C. The conclusion is that τ_r decreases with increasing air temperature: a warmer droplet simply exchanges vapor with its environment more rapidly than a cooler one (Bohren, 1987, p. 20). Mathematically, the effect manifests through the $e_{sat}(T_a)$ term in (2.1) and (2.9).

The largest τ_r values depicted in Fig. 8 are many hours. The natural environment, however, is unlikely to remain constant this long. And even if the environment does remain constant, the largest droplets are even more unlikely to stay suspended in the air long enough to approach equilibrium.

We can estimate atmospheric residence times by computing the Stokes fall speed (u_f) of each droplet. An expression for that fall speed as a function of the initial droplet radius is (Andreas, 1989)

$$u_f = \frac{2r_0^2 g}{9\nu_a[1+0.158(2r_0 u_f/\nu_a)^{2/3}]}\left(\frac{\rho_s}{\rho_a}-1\right). \quad (5.1)$$

Here g is the acceleration of gravity, and ν_a is the kinematic viscosity of air. Solving (5.1) for u_f as a function of r_0 by Newton's method is routine.

To put the effect of this gravitational settling in the context of the time constants τ_T and τ_r, let us define a residence (falling) time scale τ_f as the time required for a droplet of radius r_0 to fall 1 m in still air. That is,

$$\tau_f = 1/u_f. \quad (5.2)$$

In Fig. 9, we compare τ_T and τ_r values with the τ_f values computed from (5.1) and (5.2). We see that residence times for the largest droplets, especially, can be very short. Many of the

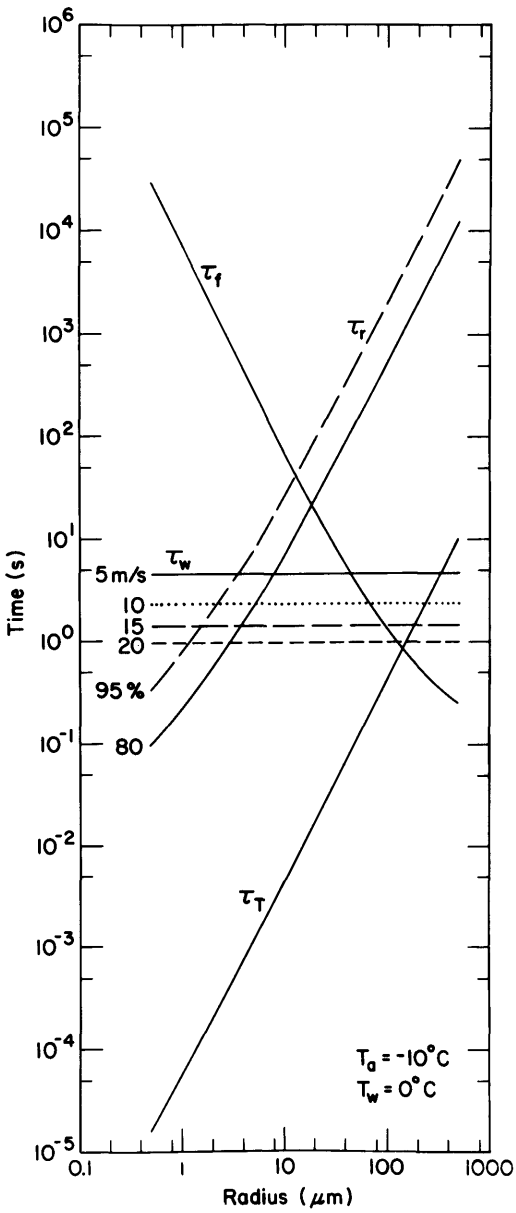

Fig. 9. A comparison of the time constants for thermal (τ_T) and moisture (τ_r) exchange with the times required for a droplet to fall 1 m in still air (τ_f) and to be lifted 1 m by a turbulent eddy (τ_w). The identifiers on τ_r are the relative humidity; on τ_w, the 10-m wind speed. Environmental conditions are $T_w = 0°C$, $T_a = -10°C$, $S = 34‰$, and $P = 1000$ hPa. The relative humidity is unimportant in specifying τ_T, τ_f, and τ_w.

droplets with radii greater than 20 μm will thus fall back into the sea before reaching their equilibrium radius: $\tau_r > \tau_f$ for these. Because of the rapidity of the thermal exchange, however, all but the very largest spray droplets should reach thermal equilibrium before falling back to the surface: that is, $\tau_f > \tau_T$, generally.

The implications of these gravitational settling times must be qualitatively correct for the smallest and largest droplets. According to Fig. 9, the smallest droplets essentially remain in the air indefinitely, and the largest droplets fall back into the sea almost immediately. Strict gravitational settling, however, is probably not a useful concept for mid-range droplets. In still air, bursting bubbles eject jet droplets to no more than 0.2 m above the water surface (Blanchard, 1963, 1989; Bortkovskii, 1987). The turbulent air, however, surely lifts some of these to greater heights. The spray droplet profiles that de Leeuw (1986a, 1986b, 1987) measured over the open ocean are evidence of this turbulent mixing. His profiles show very little decrease in droplet concentration from the surface (actually a height of 0.2 m) to heights of 10–20 m for droplets with radii less than 50 μm, the maximum size he could observe. We try to parameterize the effects of this turbulence.

Fluctuations in the vertical velocity component w in the near-surface air will suspend sea spray droplets and carry them to higher levels. We model the root-mean-square (rms) vertical velocity fluctuation $w_{rms} = (\overline{w^2})^{1/2}$, where the overbar indicates time averaging, using a relation derived experimentally by Andreas and Paulson (1979),

$$w_{rms}/u_* = 1.34 \tanh[0.66 \log(\mathrm{Re}) - 1.9]. \quad (5.3)$$

This is valid for $\mathrm{Re} > 10^4$, where, $\mathrm{Re} = U(z)\,z/\nu_a$ is the Reynolds number based on the observation height z, and $U(z)$ is the average wind speed at z. u_* is the so-called friction velocity, a fundamental velocity scale. Wu (1979, 1982) and Bortkovskii (1987) have also suggested parameterizing turbulence effects on sea spray with u_*. Although there are many expressions for w_{rms}/u_* in the literature, (5.3) seems appropriate here because it was derived from turbulence measurements over water at heights generally below 0.15 m. Remember, the maximum ejection height for jet droplets is 0.2 m.

To solve (5.3) for w_{rms} as a function of the 10-m wind speed U_{10}, we resort to the flux-gradient relations. These predict the wind speed U, air temperature T_a, and water vapor density Q_a (absolute humidity) in the atmospheric surface layer as functions of the height z and the Obukhov length L:

$$U(z) = (u_*/\kappa)[\ln(z/z_0) - \psi_m(z/L)], \quad (5.4a)$$

$$T_a(z) = T_w + (t_*/\kappa)[\ln(z/z_T) - \psi_h(z/L)], \quad (5.4b)$$

$$Q_a(z) = Q_w + (q_*/\kappa)[\ln(z/z_Q) - \psi_h(z/L)]. \quad (5.4c)$$

In these, κ is the von Kármán constant; t_* and q_* are temperature and humidity scales analogous to u_*; Q_w is the water vapor density at the sea surface, computed by assuming that the surface air is saturated at temperature T_w; z_0, z_T, and z_Q are the so-called roughness lengths for wind speed, temperature, and humidity; and ψ_m and ψ_h are the stability corrections given by Large and Pond (1982).

We can find z_0 from the neutral-stability drag coefficient referenced to 10 m, C_{DN10}, measured by Large and Pond (1981),

$$10^3\, C_{DN10} = 1.20 \quad \text{for } 4 \leqslant U_{10} < 11 \text{ m/s}, \quad (5.5a)$$

$$= 0.49 + 0.065\, U_{10} \quad \text{for } 11 \leqslant U_{10} \leqslant 25 \text{ m/s}. \quad (5.5b)$$

Because at neutral stability (5.4a) gives

$$C_{DN10}^{-1/2} \equiv U_{10}/u_* = \kappa^{-1} \ln(10/z_0), \quad (5.6)$$

we can find z_0 easily using (5.5). By specifying the neutral-stability, 10-m transfer coefficients for sensible (C_{HN10}) and latent (C_{EN10}) heat, which we take to be (Andreas and Murphy, 1986; Smith, 1988)

$$C_{HN10} = C_{EN10} = 1.0 \times 10^{-3}, \quad (5.7)$$

we can similarly compute z_T and z_Q. Andreas and Murphy (1986) gave the appropriate equations.

To use (5.3–5.7) to estimate w_{rms}, we specify T_w, and the wind speed, air temperature, and relative humidity at a height of 10 m, and then solve (5.4) iteratively for u_*, t_*, q_*, and L. We next choose $z = 0.2$ m as the height at which to estimate w_{rms} and use (5.4a) to compute $U(0.2)$. With this value, we compute Re and then use (5.3) to find w_{rms}. If w_{rms} is much less than u_f,

turbulence will probably not affect the settling of sea spray droplets very much. But if w_{rms} is equal to or larger than u_f, turbulence may well suspend the spray droplets indefinitely.

To compare the effects of the turbulence with the thermodynamic and gravitational effects, we define a time scale τ_w as

$$\tau_w = 1/w_{rms}. \tag{5.8}$$

As with τ_f in (5.2), τ_w is the time required for a spray droplet imbedded in a turbulent eddy with vertical velocity w_{rms} to travel 1 m vertically. Fig. 9 shows τ_w for several values of the 10-m wind speed. τ_w values are typically 1–5 s.

When $\tau_w \approx \tau_f$, we would need a time-dependent model to evaluate turbulence effects on droplet residence times because of the droplet inertia. But for $\tau_w < \tau_f$ and for $\tau_w > \tau_f$, our simple analysis yields fairly clear results. $\tau_w < \tau_f$ for spray droplets with initial radii less than about 40 μm. Because these droplets are light and responsive, the turbulence should be capable of suspending them, at least for a short time. $\tau_w > \tau_f$ for droplets larger than about 200 μm; these are probably too massive to be affected much by the turbulence and, thus, have a residence time of roughly τ_f. We also see from Fig. 9 that these large droplets will experience negligible moisture exchange and incomplete thermal exchange during their brief flights above the sea surface.

Figs. 5 and 9 help us identify the size of sea spray droplets that we must focus on to understand how spray affects air–sea heat and moisture transfer. We see from Fig. 9 that droplets with radii less than about 10 μm remain in the air long enough to transfer all the heat and moisture that they can because their fall speeds are so small. Droplets with radii between 10 and 40 μm may also contribute substantially to the air–sea exchange because high winds produce them in large numbers and because even a moderate wind will suspend them for a time against gravitational settling. We do not know yet, however, whether the turbulence can increase their residence times by the two orders of magnitude they need to reach moisture equilibrium. For droplets with radii between 40 and 300 μm, τ_f and τ_w are of comparable size and both are 2–3 orders of magnitude less than τ_r. Although droplets in this range will probably reach thermal equilibrium, few will likely reach moisture equilibrium. Knowing that in high winds the peak in the volume flux is associated with droplets with radii between 20 and 300 μm (Fig. 5), it is, nevertheless, crucial for us to look more closely at the effects of turbulence on these droplets.

6. Conclusions

The equations presented in Section 2 constitute a useful model for treating many problems related to the evolution of sea spray droplets. Here we have focused on the thermal and moisture evolution of spray droplets and have computed the time constants τ_T and τ_r that parameterize this evolution. τ_r is always 2–3 orders of magnitude greater than τ_T for typical humidities over the ocean. Consequently, the ambient relative humidity has negligible effect on the thermal evolution of spray droplets, and the air–sea temperature difference has minimal impact on their moisture evolution.

We also compared τ_T and τ_r with time scales that model the effects of gravitational settling (τ_f) and turbulent suspension (τ_w). Droplets of radius 10 μm and less will almost certainly reach thermal and moisture equilibrium before they fall back into the sea because both τ_T and τ_r are less than τ_f. Droplets larger than 300 μm will not alter the interfacial air–sea exchange appreciably, because both τ_T and τ_r are larger than τ_f, and τ_w is not small enough to offset the gravitational settling. In the intermediate range of droplets, 10–300 μm, the physics is more complex. For droplets between 10 and 40 μm, τ_f is still greater than τ_w; hence, turbulence will suspend these droplets for a time longer than gravitational settling would predict. They will thus reach thermal equilibrium with their environment; but τ_r is large enough in comparison to τ_f that we cannot yet say how much moisture these droplets will lose. Droplets with radii between 40 and 300 μm have comparable τ_f and τ_w values. Thus, although the τ_T values are still small enough for these droplets to reach thermal equilibrium, it is yet unclear whether they will remain in the air long enough to transfer much moisture, since the τ_r values are so large.

7. Acknowledgements

I would like to thank James H. Cragin, Austin W. Hogan, Duncan C. Blanchard,

Christopher W. Fairall, and Gerrit de Leeuw for comments on this work and Mark Hardenberg for editorial assistance. The Office of Naval Research provided support through contracts N0001486MP67847, N0001488WM22012, and N0001489WM22006.

8. Appendix: Nomenclature table

C_{DN10}	Drag coefficient over the ocean at neutral stability, referenced to a height of 10 m
C_{EN10}	Latent heat transfer coefficient over the ocean at neutral stability, referenced to a height of 10 m
C_{HN10}	Sensible heat transfer coefficient over the ocean at neutral stability, referenced to a height of 10 m
c_{ps}	4.0×10^3 J kg^{-1} °C^{-1}, the specific heat of a spray droplet (i.e., of sea water) at constant pressure
dF/dr	Spray generation function; number of droplets produced at the sea surface per unit surface area per unit time per micrometre increment in initial droplet radius
dF/dr_{80}	Spray generation function when all droplets are brought to a standard relative humidity of 80%
dF_0/dr_{80}	Contribution to dF/dr_{80} from bursting bubbles; droplet sizes referenced to a standard humidity of 80%
dF_1/dr_{80}	Contribution to dF/dr_{80} from spume droplets; droplets sizes referenced to a standard humidity of 80%
D_h	1.4×10^{-7} m^2/s, molecular diffusivity of heat in sea water at 0°C
D_s	6.8×10^{-10} m^2/s, molecular diffusivity of NaCl in sea water at 0°C
D'_w	Water vapor diffusivity in air, modified for noncontinuum effects
e_{sat}	Pressure of water vapor in saturation with a plane surface of pure water
f	RH/100, fractional relative humidity
g	9.82 m/s^2, acceleration due to gravity
k'_a	Thermal conductivity of air, modified for noncontinuum effects
L	Obukhov length, a stability parameter
L_v	Latent heat of vaporization of water
M_s	58.443×10^{-3} kg/mol, molecular weight of NaCl
m_s	Mass of salt contained by a spray droplet
M_w	18.0160×10^{-3} kg/mol, molecular weight of water
P	Atmospheric pressure
Q_a	Water vapor density of ambient air
$Q_a(z)$	Average water vapor density at height z above the surface
Q_r	Water vapor density at the surface of a spray droplet
Q_w	Water vapor density at the sea surface
q_*	A water vapor flux scale
R	8.31441 J mol^{-1} K^{-1}, universal gas constant
r	Instantaneous radius of a sea spray droplet
r_{eq}	Radius of a droplet when it is in equilibrium with its environment
r_0	Initial radius of a sea spray droplet
r_{80}	Radius of a droplet when it is in equilibrium in an environment with 80% relative humidity
Re	$U(z)\,z/\nu_a$, Reynolds number appropriate at height z
RH	$100f$, relative humidity
S	Surface salinity of the ocean
T	Instantaneous droplet temperature
t	Time
T_a	Ambient air temperature
$T_a(z)$	Average air temperature at height z above the surface
T_{eq}	Temperature of a droplet when it is in thermal equilibrium with its environment
T_w	Surface temperature of the ocean, the initial droplet temperature
t_*	A temperature flux scale
$U(z)$	Average wind speed at height z above the surface
U_{10}	Average wind speed at a height of 10 m
u_f	Terminal fall speed of a spray droplet
u_*	The friction velocity, a fundamental velocity scale
w	Turbulent fluctuation in vertical velocity
w_{rms}	$(\overline{w^2})^{1/2}$, root-mean-square vertical velocity fluctuation

y A function that gives the effects of curvature and dissolved salt on the vapor pressure at the surface of a spray droplet

z Height above the mean sea surface

z_Q Roughness length for humidity

z_T Roughness length for temperature

z_0 Roughness length for wind speed

δ $(T/T_a) - 1$, see (2.2)

κ 0.4, von Kármán's constant

ν 2, the number of ions into which a NaCl molecule dissociates

ν_a Kinematic viscosity of air

ρ_a Density of air

ρ_s Solution density of a spray droplet

ρ_w Density of pure water

σ_s Surface tension of a plane, aqueous solution

τ_f Time required for a spray droplet with terminal fall speed u_f to fall 1 m in still air

τ_h Time required for the interior of a spray droplet to be everywhere within 4% of an impulsively applied surface temperature

τ_r Time required for a spray droplet to come to within e^{-1} of its equilibrium radius

τ_s Upper bound on the time required for excess salt at a droplet surface to diffuse throughout the interior of the droplet

τ_T Time required for a spray droplet to come to within e^{-1} of its equilibrium temperature

τ_w Time required for a sea spray droplet carried in a turbulent eddy with vertical velocity w_{rms} to be lifted 1 m

Φ_s Practical osmotic coefficient of NaCl dissolved in water

ψ_h Stability correction to the semi-logarithmic temperature and humidity profiles

ψ_m Stability correction to the semi-logarithmic wind speed profile

REFERENCES

Andreas, E. L. 1989. *Thermal and size evolution of sea spray droplets.* CRREL Rep. 89-11, U.S. Army Cold Regions Research and Engineering Laboratory, Hanover, N.H., 37 pp.

Andreas, E. L. and Murphy, B. 1986. Bulk transfer coefficients for heat and momentum over leads and polynyas. *J. Phys. Oceanogr. 16*, 1875–1883.

Andreas, E. L. and Paulson, C. A. 1979. Velocity spectra and cospectra and integral statistics over Arctic leads. *Q. J. R. Meteorol. Soc. 105*, 1053–1070.

Andreas, E. L., Williams, R. M. and Paulson, C. A. 1981. Observations of condensate profiles over Arctic leads with a hot-film anemometer. *Q. J. R. Meteorol. Soc. 107*, 437–460.

Blanchard, D. C. 1963. The electrification of the atmosphere by particles from bubbles in the sea. In: *Progress in oceanography* (ed. M. Sears). New York: Macmillan, 71–202.

Blanchard, D. C. 1983. The production, distribution, and bacterial enrichment of the sea-salt aerosol. In: *Air–sea exchange of gases and particles* (eds. P. S. Liss and W. G. N. Slinn). Dordrecht: D. Reidel, 407–454.

Blanchard, D. C. 1989. The size and height to which jet drops are ejected from bursting bubbles in seawater. *J. Geophys. Res. 94*, 10999–11002.

Blanchard, D. C. and Syzdek, L. D. 1988. Film drop production as a function of bubble size. *J. Geophys. Res. 93*, 3649–3654.

Bohren, C. F. 1987. *Clouds in a glass of beer.* New York: John Wiley and Sons, 195 pp.

Borisenkov, E. P. 1974. Some mechanisms of atmosphere–ocean interaction under stormy weather conditions. *Problems of the Arctic and the Antarctic 43–44*, 73–83.

Bortkovskii, R. S. 1973. On the mechanism of interaction between the ocean and the atmosphere during a storm. *Fluid Mech.—Soviet Res. 2*, 87–94.

Bortkovskii, R. S. 1987. *Air–sea exchange of heat and moisture during storms.* Dordrecht: D. Reidel, 194 pp.

Burk, S. D. 1984. The generation, turbulent transfer and deposition of the sea-salt aerosol. *J. Atmos. Sci. 41*, 3040–3051.

Carslaw, H. S. and Jaeger, J. C. 1959. *Conduction of heat in solids*, 2nd Edition. London: Oxford University Press, 510 pp.

Cheng, R. J., Blanchard, D. C. and Cipriano, R. J. 1988. The formation of hollow sea-salt particles from the evaporation of drops of seawater. *Atmos. Res. 22*, 15–25.

Cipriano, R. J. and Blanchard, D. C. 1981. Bubble and aerosol spectra produced by a laboratory 'breaking wave'. *J. Geophys. Res. 86*, 8085–8092.

De Leeuw, G. 1986a. Size distribution of giant aerosol particles close above sea level. *J. Aerosol Sci. 17*, 293–296.

De Leeuw, G. 1986b. Vertical profiles of giant particles close above the sea surface. *Tellus 38B*, 51–61.

De Leeuw, G. 1987. Near-surface particle size distribution profiles over the North Sea. *J. Geophys. Res. 92*, 14631–14635.

De Leeuw, G. 1989. Investigations on turbulent fluctuations of particle concentrations and relative humidity in the marine atmospheric surface layer. *J. Geophys. Res. 94*, 3261–3269.

El Golli, S., Bricard, J., Turpin, P.-Y. and Treiner, C. 1974. The evaporation of saline droplets. *J. Aerosol Sci. 5*, 273–292.

Emanuel, K. A. and Rotunno, R. 1989. Polar lows as Arctic hurricanes. *Tellus 41A*, 1–17.

Fairall, C. W., Davidson, K. L. and Schacher, G. E. 1983. An analysis of the surface production of sea-salt aerosols. *Tellus 35B*, 31–39.

Fitzgerald, J. W. 1975. Approximation formulas for the equlibrium size of an aerosol particle as a function of its dry size and composition and the ambient relative humidity. *J. Appl. Meteorol. 14*, 1044–1049.

Horne, R. A. 1969. *Marine chemistry*. New York: Wiley-Interscience, 568 pp.

Kellogg, W. W. and Twitchell, P. F. 1986. Summary of the Workshop on Arctic Lows, 9–10 May 1985, Boulder, Colorado. *Bull. Amer. Meteorol. Soc. 67*, 186–193.

Lai, R. J. and Shemdin, O. H. 1974. Laboratory study of the generation of spray over water. *J. Geophys. Res. 79*, 3055–3063.

Large, W. G. and Pond, S. 1981. Open ocean momentum flux measurements in moderate to strong winds. *J. Phys. Oceanogr. 11*, 324–336.

Large, W. G. and Pond, S. 1982. Sensible and latent heat flux measurements over the ocean. *J. Phys. Oceanogr. 12*, 464–482.

Ling, S. C. and Kao, T. W. 1976. Parameterization of the moisture and heat transfer process over the ocean under whitecap sea states. *J. Phys. Oceanogr. 6*, 306–315.

Ling, S. C., Saad, A. and Kao, T. W. 1978. Mechanics of multiphase fluxes over the ocean. In: *Turbulent fluxes through the sea surface, wave dynamics, and prediction* (eds. A. Favre and K. Hasselmann). New York: Plenum Press, 185–194.

Mestayer, P. and Lefauconnier, C. 1988. Spray droplet generation, transport, and evaporation in a wind wave tunnel during the Humidity Exchange over the Sea Experiments in the Simulation Tunnel. *J. Geophys. Res. 93*, 572–586.

Mestayer, P. G., Edson, J. B., Fairall, C. W., Larsen, S. E. and Spiel, D. E. 1989. Turbulent transport and evaporation of droplets generated at an air–water interface. In: *Turbulent Shear Flows 6* (eds. J.-C. André, J. Cousteix, F. Durst, B. E. Launder, F. W. Schmidt and J. H. Whitelaw). Berlin: Springer-Verlag, 129–147.

Monahan, E. C. 1968. Sea spray as a function of low elevation wind speed. *J. Geophys. Res. 73*, 1127–1137.

Monahan, E. C., Davidson, K. L. and Spiel, D. E. 1982. Whitecap aerosol productivity deduced from simulation tank measurements. *J. Geophys. Res. 87*, 8898–8904.

Monahan, E. C., Fairall, C. W., Davidson, K. L. and Boyle, P. J. 1983. Observed inter-relations between 10 m winds, ocean whitecaps and marine aerosols. *Q. J. R. Meteorol. Soc. 109*, 379–392.

Monahan, E. C., Spiel, D. E. and Davidson, K. L. 1986. A model of marine aerosol generation via whitecaps and wave disruption. In: *Oceanic whitecaps and their role in air–sea exchange processes* (eds. E. C. Monahan and G. Mac Niocaill). Dordrecht: D. Reidel, 167–174.

Preobrazhenskii, L. Yu. 1973. Estimate of the content of spray-drops in the near-water layer of the atmosphere. *Fluid Mech.—Soviet Res. 2*, 95–100.

Pruppacher, H. R. and Klett, J. D. 1978. *Microphysics of clouds and precipitation*. Dordrecht: D. Reidel, 714 pp.

Ranz, W. E. and Marshall, W. R., Jr. 1952. Evaporation from drops. Part II. *Chem. Eng. Progress 48*, 173–180.

Rasmussen, E. 1983. A review of meso-scale disturbances in cold air masses. In: *Mesoscale meteorology—theories, observations and models* (eds. D. K. Lilly and T. Gal-Chen). Dordrecht: D. Reidel, 247–283.

Rasmussen, E. 1985. A case study of a polar low development over the Barents Sea. *Tellus 37A*, 407–418.

Rasmussen, E. and Lystad, M. 1987. The Norwegian Polar Lows Project: A summary of the International Conference on Polar Lows, 20–23 May 1986, Oslo, Norway. *Bull. Amer. Meteorol. Soc. 68*, 801–816.

Shapiro, M. A., Fedor, L. S. and Hampel, T. 1987. Research aircraft measurements of a polar low over the Norwegian Sea. *Tellus 39A*, 272–306.

Smith, S. D. 1988. Coefficients for sea surface wind stress, heat flux, and wind profiles as a function of wind speed and temperature. *J. Geophys. Res. 93*, 15467–15472.

Stramska, M. 1987. Vertical profiles of sea salt aerosol in the atmospheric surface layer: a numerical model. *Acta Geophys. Polonica 35*, 87–100.

Street, R. L., Wang, C. S., McIntosh, D. A. and Miller, A. W., Jr. 1978. Fluxes through the boundary layers at an air–water interface: laboratory studies. In: *Turbulent fluxes through the sea surface, wave dynamics, and prediction* (eds. A. Favre and K. Hasselmann). New York: Plenum Press, 99–118.

Twomey, S. 1954. The composition of hygroscopic particles in the atmosphere. *J. Meteorol. 11*, 334–338.

Wang, C. S. and Street, R. L. 1978a. Measurements of spray at an air–water interface. *Dynam. Atmos. Oceans 2*, 141–152.

Wang, C. S. and Street, R. L. 1978b. Transfer across an air–water interface at high wind speeds: the effect of spray. *J. Geophys. Res. 83*, 2959–2969.

Woolf, D. K., Bowyer, P. A. and Monahan, E. C. 1987. Discriminating between the film drops and jet drops produced by a simulated whitecap. *J. Geophys. Res. 92*, 5142–5150.

Wu, J. 1973. Spray in the atmospheric surface layer: laboratory study. *J. Geophys. Res. 78*, 511–519.

Wu, J. 1974. Evaporation due to spray. *J. Geophys. Res. 79*, 4107–4109.

Wu, J. 1979. Spray in the atmospheric surface layer: review and analysis of laboratory and oceanic results. *J. Geophys. Res. 84*, 1693–1704.

Wu, J. 1982. Sea spray: a further look. *J. Geophys. Res. 87*, 8905–8912.

Wu, J., Murray, J. J. and Lai, R. J. 1984. Production and distributions of sea spray. *J. Geophys. Res. 89*, 8163–8169.